Proceedings of the 4th International Conference on Energy Sustainability
ES2010
May 17-22, 2010, Phoenix, Arizona, USA

ES2010-90053

METHODOLOGY TO ASSESS POTENTIAL GLINT AND GLARE HAZARDS FROM CONCENTRATING SOLAR POWER PLANTS: ANALYTICAL MODELS AND EXPERIMENTAL VALIDATION

Clifford K. Ho, Cheryl M. Ghanbari, and Richard B. Diver
Concentrating Solar Technologies Department, Sandia National Laboratories, P.O. Box, 5800, Albuquerque, NM 87185-1127, USA, (505) 844-2384, ckho@sandia.gov

ABSTRACT

With growing numbers of concentrating solar power systems being designed and developed, glint and glare from concentrating solar collectors and receivers is receiving increased attention as a potential hazard or distraction for motorists, pilots, and pedestrians. This paper provides analytical methods to evaluate the irradiance originating from specularly and diffusely reflecting sources as a function of distance and characteristics of the source. Sample problems are provided for both specular and diffuse sources, and validation of the models is performed via testing. In addition, a summary of safety metrics is compiled from the literature to evaluate the potential hazards of calculated irradiances from glint and glare. Previous safety metrics have focused on prevention of permanent eye damage (e.g., retinal burn). New metrics used in this paper account for temporary flash blindness, which can occur at irradiance values several orders of magnitude lower than the irradiance values required for irreversible eye damage.

1. INTRODUCTION

Assessment of the potential hazards of glint and glare from concentrating solar power plants is an important requirement to ensure public safety [1]-[3]. Glint is defined as a momentary flash of light, while glare is defined as a more continuous source of excessive brightness relative to the ambient lighting. Hazards from glint and glare from concentrating solar power plants include the potential for permanent eye injury (e.g., retinal burn) and temporary disability or distractions (e.g., flash blindness), which may impact people working nearby, pilots flying overhead, or motorists driving alongside the site.

Applications and certifications for solar thermal power plants require an assessment of "visual resources" at the site (e.g., [4]-[8]), but rigorous and uniform treatment of glint and glare are lacking. Several previous studies [1]-[3] investigated the impact of specular reflections using permanent eye damage as a metric. The purpose of this paper is to provide a general assessment method that can be used to evaluate potential hazards of glint and glare for all of the primary concentrating solar power (CSP) technologies: (1) power tower systems, (2) linear concentrator systems (e.g., parabolic troughs, linear Fresnel), and (3) dish/engine systems. In particular, this paper provides analytical solutions to evaluate the irradiance originating from both specularly and diffusely reflecting sources as a function of distance and characteristics of the source. In addition, tests were conducted at the National Solar Thermal Test Facility (NSTTF) at Sandia National Laboratories to validate the models. Modeling results (analytical and ray-tracing) were compared to the data, which showed excellent agreement. The measured and/or calculated irradiances can be compared against the compiled safety metrics to determine safe perimeter zones or regions where personal protective equipment may be needed.

2. REVIEW OF OCULAR SAFETY METRICS

This section summarizes the ocular safety metrics introduced in Ho et al. [9]. Figure 1 summarizes the potential impact of different retinal irradiances as a function of subtended source angle for a 0.15 s exposure. Three regions are shown: (1) potential for permanent eye damage (retinal burn), (2) potential for temporary after-image (flash blindness), and (3) low potential for temporary after-image. If the retinal irradiance is sufficiently large for a given subtended source angle, permanent eye damage from retinal burn may occur [3],[11]. Note that as the subtended source angle increases, the safe retinal irradiance threshold decreases because of the increased size of the retinal image area, and, hence, increased energy applied to the retina. Brumleve provides a lower

 Copyright © 2010 by ASME

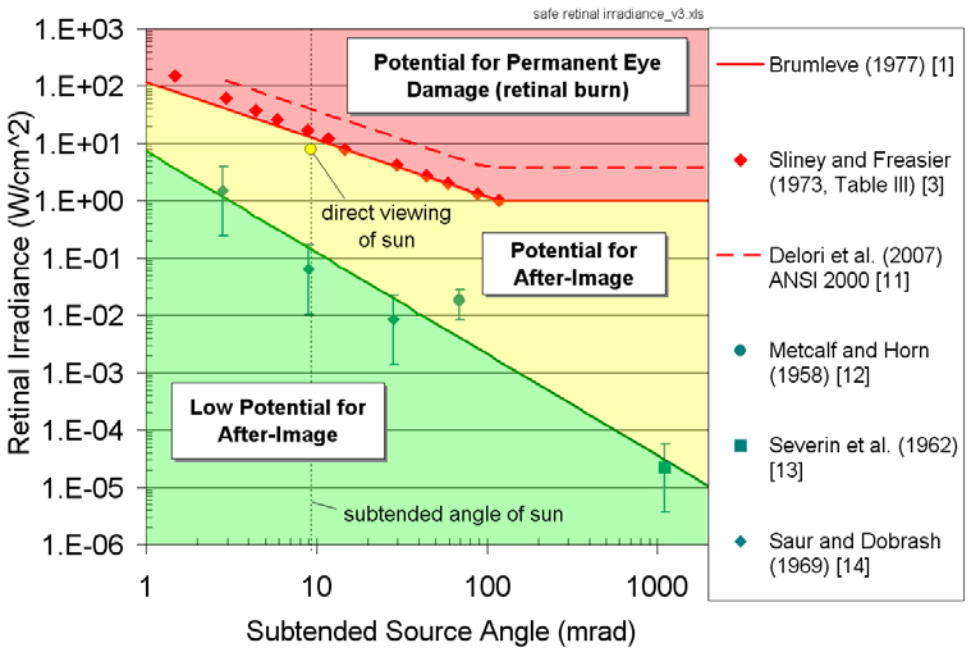

Figure 1. Potential impacts of retinal irradiance as a function of subtended source angle for 0.15 s exposure (typical blink response time). Data for irreversible eye damage is from [1], [10], and [11]. Data for temporary flash blindness (after-image) is from [12], [13], and [14].

threshold for the retinal irradiance corresponding to permanent eye damage using data from [3]:

$$E_{r,burn} = 0.118 / \omega \quad \text{for } \omega < 0.118 \text{ rad} \tag{1}$$

$$E_{r,burn} = 1 \quad \text{for } \omega \geq 0.118 \text{ rad} \tag{2}$$

where $E_{r,burn}$ is the retinal burn threshold [W/cm^2] and ω is the subtended angle [rad]. Below the retinal burn threshold, a region exists where a sufficiently high retinal irradiance may cause temporary flash blindness, which is caused by bleaching (oversaturation) of the retinal visual pigments [3]. When this occurs, a temporary after-image appears in the visual field (e.g., the effect after viewing a camera flash in a dim room). The size and impact of the after-image in the field of view depends on the size of the subtended source angle. For a given retinal irradiance, smaller source angles yield smaller after-images, and the potential impact is less. In Figure 1, data from [12]-[14] were used to fit a lower threshold for potential after-image effects. In [12]-[14], people were subjected to different source luminances, and their recovery time was recorded. The minimal retinal irradiance based on the illuminance[1] and subtended source angle that yielded at least one second of after-image is shown in Figure 1. Error bars represent uncertainty in the pupil diameter (2 – 8 mm) [13],[14] and variability in subject response [12]. A fit corresponding to these data that yielded the minimal retinal irradiances that caused an after-image is as follows:

$$E_{r,\,flash} = \frac{3.59\text{x}10^{-5}}{\omega^{1.77}} \tag{3}$$

where $E_{r,flash}$ is the threshold for potential after-image [W/cm^2] and ω is the subtended source angle [rad]. Values of retinal irradiance below $E_{r,flash}$ have a low potential for after-image impact. Note that, as plotted in Figure 1, a brief direct viewing of the sun (0.15 s) has a high potential for after-image effects, but it has a low potential for permanent eye damage.

The retinal irradiance (power per unit area) can be calculated from the total power entering the pupil and the retinal image area. The diameter, d_r, of the image projected onto the retina (assuming circular images) can be determined from the source angle (ω), which can be calculated from the source size (d_s), radial distance (r) between the eye and the source, and the focal length of the eye ($f \cong 0.017$ m), as follows:

$$d_r = f\,\omega$$

$$\text{where } \omega = d_s / r \tag{4}$$

Eq. (4) assumes that the arc and the chord of a circle are the same for small angles. At a source angle, ω, of 60°, the error in d_r is ~5%. If the irradiance at a plane in front of the cornea, E_c (W/m^2), is known, the power entering the pupil can be calculated as the product of the irradiance and the pupil area

[1] The ratio of solar illuminance to solar irradiance at the earth's surface yields a conversion factor of ~100 lumens/W.

Copyright © 2010 by ASME

(the diameter of the pupil, d_p, adjusted to sunlight is ~2 mm). The power is then divided by the retinal image area and multiplied by a transmission coefficient, τ (~0.5) [10], for the ocular media (to account for absorption of radiation within the eye before it reaches the retina) to yield the following expression for the retinal irradiance:

$$E_r = E_c \left(\frac{d_p^2}{d_r^2} \right) \tau \tag{5}$$

It should be noted that Brumleve [1] includes an additional coefficient (ν) to account for the fraction of solar irradiance between 400 and 1400 nm, but this has been included in the transmission coefficient, τ, above. As an example, the retinal irradiance caused by viewing the sun directly can be calculated using Eqs. (4) and (5) with E_c = 0.1 W/cm^2, d_p = 0.002 m, f = 0.017 m, ω = 0.0093 rad, and τ = 0.5, which yields a retinal irradiance, E_r, of ~8 W/cm^2. Note that the retinal irradiance is significantly higher than the irradiance at the entrance of the eye.

3. MODELING APPROACH

This section presents analytical methods for calculating irradiance caused by specular and diffuse reflections of sunlight as a function of distance and other characteristics of the source. Specular reflections occur from polished mirror-like surfaces so that the reflected angle is equal to the incident angle relative to the surface normal. Diffuse reflections occur from uneven or rough surfaces that scatter the incident radiation such that the radiance (intensity) is uniform in all directions (see Figure 2). The following sections provide methods to calculate the irradiance from specular and diffuse reflections. Once the irradiance is determined, the equations in the previous section can be used to calculate the retinal irradiance for comparison against the safe retinal irradiance metrics presented in Figure 1.

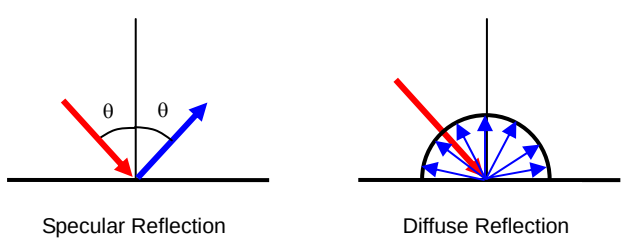

Figure 2. Illustration of specular versus diffuse reflections.

3.1 Analytical Model of Specular Reflections

Direct specular solar reflection from mirrors can cause glint and glare hazards when heliostats are in standby positions (reflecting the sun at locations other than the receiver). Specular solar reflections from dishes and parabolic troughs can cause glint and glare hazards when the collectors are in off-axis positions (e.g., when moving from a stowed position to a tracking position). For parabolic troughs, glint and glare from specular reflections can also occur when the sun is low in the horizon and aligned with the axis of the trough, causing reflected rays to spill from the end of the trough.

3.1.1 Point-Focus Collectors

An analytical model of beam irradiance resulting from specular solar reflections from a point-focus mirror has been derived [1] with the following assumptions (see Figure 3):

- Uniform sun intensity (no limb darkening)
- Round, focused, continuous surface mirrors
- No cosine losses, off-axis aberrations, or atmospheric attenuation
- Uniform intensity in beam cross section

The assumptions above will generally produce the largest beam irradiance, but the assumption of uniform sun intensity averages the intensity over the entire beam. Using a non-uniform solar intensity creates larger peak fluxes towards the center of the beam. Comparisons with a ray-tracing model (ASAP®) show that the difference in peak flux is about 25-30% at the focal length, but the difference can be greater at other distances.

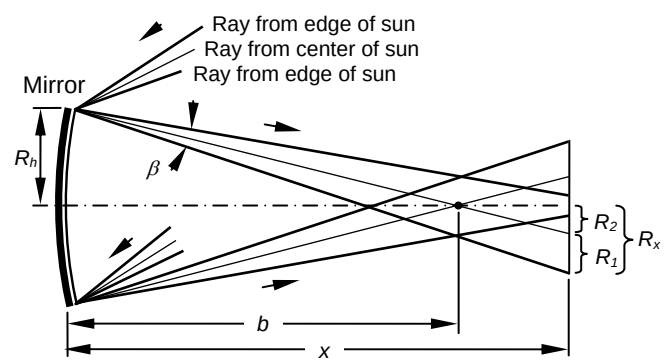

Figure 3. Geometry of specular solar reflections from a focused mirror where *b* is the focal length, R_h is the radius of the mirror, β is the beam divergence angle, and R_x is the radius of the beam cross section at distance, *x*, from the mirror (adapted from [1]).

The beam irradiance, I [W/cm^2], is then calculated as the product of the direct normal insolation, Q [W/cm^2], the mirror reflectivity, ρ [-], and the area concentration ratio, C [-]:

$$I = \rho Q C \tag{6}$$

The direct normal insolation, Q, at the earth's surface is approximately 0.1 W/cm^2. The area concentration ratio, C, can be calculated as follows assuming a circular mirror area, A_h, with radius, R_h, and a circular beam area, A_x, with radius, R_x, at a distance, x, from the mirror:

Copyright © 2010 by ASME

$$C = \frac{A_h}{A_x} = \left(\frac{R_h}{R_x}\right)^2 \tag{7}$$

The radius, R_x, of the beam is comprised of two components:

$$R_x = R_1 + R_2 \tag{8}$$

where R_1 is caused by the sun angle and mirror contour inaccuracies (slope error) and R_2 represents the focusing and defocusing characteristics of the beam at a distance that is less than or greater than the focal length. The beam divergence, R_1, at a distance, x, from the mirror is defined by the sun half-angle (4.7 mrad) and any additional slope errors caused by mirror inaccuracies:

$$R_1 \approx x \tan\left(\frac{\beta}{2}\right) \tag{9}$$

where $\beta/2$ is the half-angle [rad] of the total beam divergence. According to [1], this approximation has an error that is less than 0.3% for $b/R_h > 18$. R_2 can be defined using similar triangles as shown in Figure 3, where b is the focal length:

$$\frac{R_2}{|x-b|} = \frac{R_h}{b}$$

$$\Rightarrow R_2 = \left|\frac{x}{b} - 1\right| R_h \tag{10}$$

Using Eqs. (7), (8), (9), and (10) in Eq. (6), and the approximation that $\tan(\beta/2) = \beta/2$ when $\beta/2$ is small, yields the following expression for the beam irradiance [W/cm^2]:

$$I = \rho Q \left(\frac{x\beta}{D_h} + \left|\frac{x}{b} - 1\right|\right)^{-2} \text{ (point-focus collectors)} \tag{11}$$

where $D_h = 2\,R_h$. The beam irradiance can also be presented in units of "suns" by dividing Eq. (11) by Q (~0.1 W/cm^2). The maximum beam irradiance occurs at the focal length, $x = b$. In addition, the beam irradiance from a flat mirror can be calculated by setting $b = \infty$ in Eq. (11). The specular beam irradiance for several focal lengths is plotted in Figure 4 as a function of distance, x, from the mirror. The reflectivity, ρ, is assumed to be 0.92, and the total beam divergence angle, β, is assumed to be equal to 9.4 mrad. The effective diameter of the mirror, D_h, is calculated from the total mirrored area (37 m^2) of individual heliostats used at the National Solar Thermal Test Facility at Sandia National Laboratories in Albuquerque, NM:

$$D_h = \left(\frac{4A_h}{\pi}\right)^{0.5} \tag{12}$$

As defined in Eq. (6), the irradiance is proportional to the concentration ratio, which is equal to the ratio of the measured irradiance at a given distance and the product of the direct normal insolation, Q, and the mirror reflectivity. The concentration ratio is also equal to the area ratio of the mirror and the beam size. It follows that the relative spot size of the reflected image of the sun in the mirror at a given distance is proportional to the measured irradiance at that location. Once the irradiance, I, is determined, the spot size of the reflected image of the sun in the mirror can be estimated by the following equation assuming that the spot size is proportional to the irradiance:

$$\frac{A_{spot}}{A_o} = \left(\frac{d_{spot}}{d_o}\right)^2 = \left(\frac{x\omega_{spot}}{x\beta}\right)^2 = C = \frac{I}{\rho Q}$$

$$\Rightarrow \quad \omega_{spot} = \beta\sqrt{\frac{I}{\rho Q}} \tag{13}$$

where A is the area of the reflected image on the mirror as viewed by an observer a distance, x, away from the mirror, d is the diameter of the reflected image on the mirror, ω is the subtended angle of the reflected sun image on the mirror (sun angle plus slope error) as observed from a prescribed distance, β is the beam divergence angle (sun angle plus slope error), the subscript "*spot*" refers to the observed spot image on the mirror, and the subscript "*o*" refers to a nominal spot image of the sun at an irradiance of one sun times the mirror reflectivity (ρQ). Thus, if the measured irradiance, I, is greater (or less) than ρQ, the observed size and subtended angle, ω_{spot}, of the reflected spot image of the sun will be greater (or less) than the nominal size and subtended angle, β, of the reflected sun image (e.g., ~9.4 mrad plus slope error) at a location, x.

Using Eq. (13) in Eqs. (4) and (5) yields the following expression for the retinal irradiance, where the corneal irradiance, E_c, is set equal to the irradiance, I, used in Eqs. (11) and (13):

$$E_r = \frac{\rho Q d_p^2 \tau}{f^2 \beta^2} \tag{14}$$

Note that the retinal irradiance in Eq. (14) does not depend on distance from the source (assuming no atmospheric attenuation). As distance increases, both the power entering the pupil and the retinal image area (which is proportional to the square of the subtended source angle) decrease at the same rate. Therefore, the retinal irradiance, which is equal to the power entering the pupil divided by the retinal image area, is independent of distance (assuming no atmospheric attenuation). The corneal irradiance, however, changes as a function of distance as given by Eq. (11).

The plots in Figure 4 represent corneal irradiance values (at front of the eye) that could be experienced at different distances and for mirrors of different focal lengths but with prescribed reflectivity, beam divergence angle, and effective mirror size. Eqs. (11) and (12) can be used to determine the beam irradiance (I, which is equivalent to E_c in Eq. (5)) for other mirror characteristics, and then Eqs. (4) and (5) can be

Copyright © 2010 by ASME

used to determine the equivalent retinal irradiance for comparison against the safe retinal irradiance metrics in Figure 1. For example, at a distance of 200 m, the irradiance from a mirror with a focal length of 100 m and the prescribed optical characteristics is approximately 0.057 W/cm^2 according to Figure 4 and Eq. (11). To convert this "corneal irradiance" to a retinal irradiance, Eqs. (4) and (5) are used where the subtended angle, ω, in Eq. (4) is taken from the subtended angle, ω_{spot}, calculated in Eq. (13) to be 7.4 mrad for ρ=0.92, Q=0.1 W/cm^2, and β=9.4 mrad. The retinal irradiance is then found to be 7.2 W/cm^2 with d_p = 0.002 m, f = 0.017 m, and τ = 0.5 (Eq. (14) yields the same value). According to Figure 1, at a subtended source angle of 7.4 mrad, the calculated retinal irradiance of 7.2 W/cm^2 will not produce permanent eye damage. However, the calculated irradiance is sufficient to potentially cause a temporary after-image if one were to view directly at the source. The minimum distance to yield a low potential for after-image in this example is calculated to be ~910 m using Eqs. (3), (11), and (13).

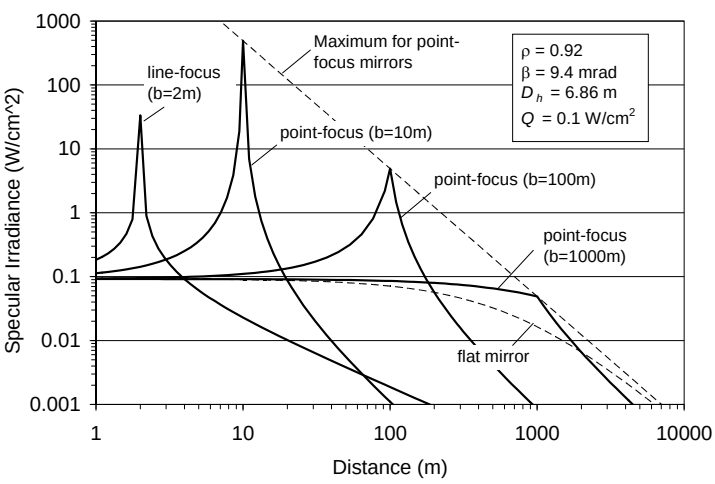

Figure 4. Specular irradiance at the cornea as a function of distance from point-focus and line-focus mirrors with different focal lengths (b) for a solar irradiance at the surface of the earth of 0.1 W/cm^2.

3.1.2 Line-Focus Collectors

The equations derived in the previous section for determining the specular beam irradiance from point-focus collectors can be readily extended to line-focus (parabolic trough, linear Fresnel) collectors. The primary difference is that the concentration ratio in Eq. (7) is changed since the convergence/divergence of rays caused by the shape of the line-focus mirror is primarily in one dimension (rather than two):

$$C = \frac{A_h}{A_x} = \frac{R_h}{R_x} \tag{15}$$

The resulting irradiance from specular reflections from a line-focus collector then becomes:

$$I = \rho Q \left(\frac{x\beta}{D_h} + \left| \frac{x}{b} - 1 \right| \right)^{-1} \text{(line-focus collectors)} \tag{16}$$

Eq. (16) is similar in form to Eq. (11) for point-focus collectors. However, the irradiance from line-focus collectors decreases less rapidly with distance past the focal point. Figure 4 shows the specular irradiance from a line-focus collector as a function of distance with an assumed focal length of 2 m, an aperture of 6.86 m, and characteristics as shown in the plot.

The equation that was used to calculate the spot size of the reflected image for point-focus mirrors (Eq. (13)) is still valid to describe the spot size of the reflected sun image in the line-focus mirror. Then, using Eqs. (13) and (16) in Eqs. (4) and (5) yields the same expression for the retinal irradiance as Eq. (14) for point-focus collectors. The retinal irradiance is independent of distance (assuming no atmospheric attenuation) because the retinal image area decreases at the same rate as the irradiance (albeit at a slower rate for line-focus mirrors than for point-focus mirrors); therefore, the retinal irradiance (power entering the eye divided by the retinal image area) is constant.

For the characteristics of a line-focus (trough) collector shown in Figure 2, the specular irradiance at a distance of 100 m is 1.87x10^{-3} W/cm^2 (Eq. (16)). The corresponding subtended source angle is 1.34 mrad (Eq. (13)) and the retinal irradiance is 7.2 W/cm^2 (Eq. (14)). According to Figure 1 and Eq. (3), this retinal irradiance and subtended source angle will not yield permanent eye damage, but there is a potential for after-image effects if one were to view the specular reflection directly. For this example, the minimum distance to yield a low potential for after-image effects is ~170 m using Eqs. (3), (13), and (16).

3.2 Analytical Model of Diffuse Reflections

Reflections from receivers, which are used to absorb the concentrated solar flux from heliostat, dish, and trough collector systems, can be modeled as diffuse rather than specular. Calculation of the irradiance at a location resulting from diffuse reflections depends on the total flux received by the reflecting source, reflectivity, size, and position of the source, and distance to the source. First, the total power, P_d (W), emanating diffusely from the source is determined as follows:

$$P_d = (DNI)\, C\left(A_d\right) \rho \tag{17}$$

where DNI is the direct normal insolation (W/m^2), C is the concentration ratio (Eq. (7)), A_d is the surface area of the diffuse source (m^2), and ρ is the reflectivity of the diffuse source. For a diffuse source, we assume that the reflected radiance is uniform in all directions, yielding the following equation for diffuse irradiance, $I_{,d}$ (W/m^2) as a function of

Copyright © 2010 by ASME

radial distance, r (m), for spherical or hemispherical source emission:

$$I_d = \left(\frac{P_d}{2\pi A_d}\right)\left(\frac{A_s \cos(\theta)}{r^2}\right) \text{ (diffuse, spherical emission)} \tag{18}$$

$$I_d = \left(\frac{P_d}{\pi A_d}\right)\left(\frac{A_s \cos(\theta)}{r^2}\right) \text{ (diffuse, hemispherical emission)} \tag{19}$$

where the first term on the right-hand side of Eqs. (18) and (19) is the reflected radiance [W/m^2-sr], which is equal to the emissive flux (P_d/A_d) divided by 2π (spherical) or π (hemispherical). The radiance is then multiplied by the solid angle (defined by the second term on the right-hand side of Eqs. (18) and (19)) subtended by the visible source area, A_s, as viewed by an observer a radial distance, r, away from the source, where θ is the angle between the surface normal and the line between the source and the observer. Note that as θ increases to 90°, the visible source area and the subtended solid angle go to zero. If the radiating source is planar, then $A_d = A_s$. The potential for different areas of the diffuse source arise when a non-planar source exists, such as a cylindrical external receiver. In this case, the diffuse source area, A_d, is equal to $\pi*D*H$, while the visible area, A_s, is approximately equal to $D*H$, where D is the diameter of the cylinder and H is the height. The projected area perpendicular to the line of sight is equal to $A_s\cos(\theta)$. See Figure 5 for a graphical representation of these parameters.

Combining Eq. (18) or (19) with Eqs. (4) and (5) yields the following expressions for the subtended angle, ω [rad], and diffuse retinal irradiance, $E_{r,d}$ [W/m^2], where the corneal irradiance, E_c, in Eq. (5) is set equal to the diffuse irradiance, I_d, and the source size, d_s, is determined using Eq. (12) with $A_h=A_s\cos(\theta)$:

$$\omega = \frac{\sqrt{4A_s \cos(\theta)/\pi}}{r} \tag{20}$$

$$E_{r,d} = \frac{P_d d_p^2 \tau}{8A_d f^2} \text{ (diffuse, spherical emission)} \tag{21}$$

$$E_{r,d} = \frac{P_d d_p^2 \tau}{4A_d f^2} \text{ (diffuse, hemispherical emission)} \tag{22}$$

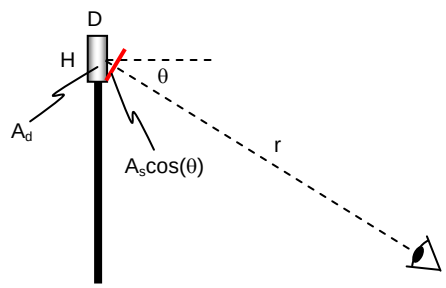

Figure 5. Illustration of parameters used for diffuse-reflection calculations (e.g., viewing an external cylindrical receiver on top of a tower).

As an example, the irradiance from a diffusely reflecting power-tower external cylindrical receiver is calculated using the following parameters:

- Flux on power-tower receiver = 1x10^6 W/m^2 (1000 suns at a DNI=1000 W/m^2)
- Radius of receiver = 10 m
- Height of receiver = 20 m
- Height of tower = 90 m
- Receiver surface area = 1,257 m^2 (calculated from receiver radius and height)
- Reflectivity of receiver = 0.1 – 0.5

Figure 6 shows a plot of the calculated corneal irradiance (at the front of the eye) as a function of distance from the receiver for reflectivity values of 0.1 and 0.5 assuming a diffuse spherical radiance (Eq. (18)). The irradiance decreases rapidly with increasing distance because the area over which the radiative power is distributed grows as a function of distance squared. Near the base of the tower at a radial distance close to 100 m (looking straight up at the receiver), the irradiance drops off to zero because the visible source area (modified by cos(θ) in Eqs. (18) and (19)) goes to zero.

The calculated irradiance can then be used to calculate the retinal irradiance (Eqs. (4) and (5)) for comparison against the safety metrics in Figure 1. For example, at a radial distance of 300 m (horizontal distance of 283 m), the irradiance from Figure 6 is 0.033 W/cm^2 at a reflectivity of 0.5. The visible area, A_s, of the receiver is 20 m x 20 m = 400 m^2, and cos(θ)=283/300=0.94. So, the projected area perpendicular to the line of sight is 400 x 0.94 = 376 m^2, and the effective diameter of an equivalent circular area is given by Eq. (12) as 21.9 m. The subtended angle of the receiver is then calculated using Eq. (4) as 21.9 m / 300 m = 0.073 rad, and the retinal image size is 1.24x10^{-3} m using f = 0.017 m. Eq. (5) then yields a retinal irradiance of 0.043 W/cm^2 using d_p = 0.002 m (Eq. (21) yields the same value). According to Figure 1 (retinal irradiance = 0.043 W/cm^2 and subtended angle = 73 mrad), this irradiance will not cause irreversible eye damage, but it is

Copyright © 2010 by ASME

sufficient to produce a temporary after-image if one looks directly at the source. The minimal safe distance to prevent a temporary after-image effect can be calculated by using Eqs. (3) and (20) to determine at what distance, *r*, the retinal irradiance (0.043 W/cm^2) is less than the after-image threshold given in Eq. (3). This distance is calculated to be approximately 1,210 m, assuming no atmospheric attenuation. This large distance is a result of the large receiver size and the large amount of incident power on the receiver (1000 suns).

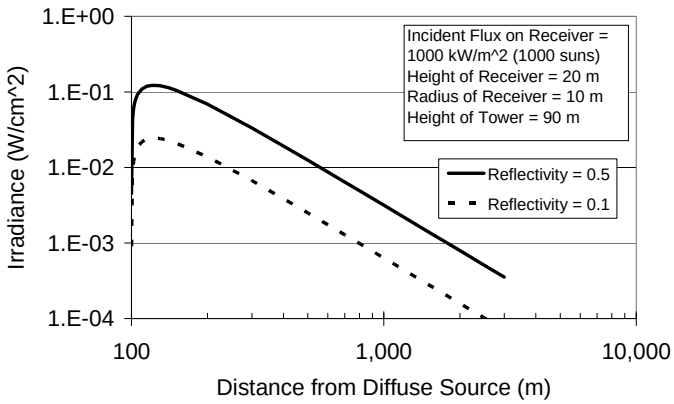

Figure 6. Irradiance at the cornea as a function of distance from a diffuse source with different reflectivities.

4. TESTING AND MODEL VALIDATION

The specular and diffuse reflection models were evaluated via testing at the National Solar Thermal Test Facility (NSTTF) at Sandia National Laboratories. Irradiances from specular reflections were evaluated by aiming a parabolic dish collector off-axis from the sun. Irradiances from diffuse reflections were evaluated from heliostat-generated beam images on the front wall of the central receiver tower at the NSTTF. A Nikon D70 digital single-lens reflex camera was used to capture the reflected images from the sun off both the parabolic dish and the tower wall at varying distances from the reflected image using f/32 and a shutter speed of 1/8000th second. Distances were recorded using a Bushnell Scout 1000 Rangefinder. Neutral density (ND) filters, which reduce the intensity of all wavelengths of light equally, were applied to the camera lens to prevent the reflections from saturating the image. The ND filters are labeled according to their attenuation factor (e.g., ND2, ND8); larger numbers indicate more attenuation and less transmittance. For example, an ND2 filter transmits 50% of the incoming light, while an ND8 filter transmits only 12.5% of the incoming light. Direct images of the sun, which were used as a reference for the reflected images, required several filters (three ND8 and an ND2), while images of the reflections required fewer filters.

MATLAB® was used to process the raw image files by summing the pixel intensity values over the region of the reflected sun image in each photo. Each pixel value was multiplied by the filter value(s) used in each image. For example, if a single ND2 filter was used, the pixel value would be multiplied by 2. The sum of the pixel values for each reflected image was divided by the sum of the pixel values for the direct sun image to yield the normalized irradiance measured in suns. These values were then compared to the predicted irradiances from the models for the specular and diffuse reflection tests.

Errors associated with the measurement of the reflected irradiance include the following: (1) uncertainty of the measured reflectivity, (2) uncertainty of the measured distance, and (3) uncertainty of the area (number of pixels) associated with the reflected sun image. The uncertainty of the measured reflectivity can be ±2-3%, depending on the location of the measurements vs. the location of the reflected sun image. The uncertainty associated with the measured distance to the reflected image is ±1-2 m. The errors associated with the image processing increase with distance from the reflected image. If the zoom is not changed, then the number of pixels used in the camera image to represent the sun is reduced. Therefore, the area representing the reflected sun image (i.e., number of pixels selected to represent the reflected sun image) becomes relatively more uncertain as the image size is reduced, and this adds to the uncertainty of the relative irradiance determined from the image processing algorithm. We estimate that the uncertainty associated with the image size is less than several percent when the reflected sun image fills the camera screen, but it can be as high as 100% or more if the reflected image is small, say, 1% of the total camera view. When comparing the cumulative pixel values from the reflected sun image to the actual sun image, one can zoom in to fill the camera screen as much as possible with the reflected sun image to reduce errors associated with the calculated area (number of pixels) associated the reflected sun image.

4.1 Specular Reflection Tests

The specular reflection tests were conducted on July 1, 2009, at approximately 9:30 AM (MDT) with a direct normal insolation of approximately 850 W/m^2. The Mod 2-2 10 kW parabolic dish used in the tests had a focal length of 5.448 m, a diameter of 8.8 m, a reflectivity of 0.93, and an estimated RMS slope error of 1 mrad [16]. The dish was positioned so that the reflected image of the sun was visible on mirror facets of the dish as the observer moved in a southerly direction away from the dish. Photos of the reflected image on the dish were taken at varying distances, and the images were processed in MATLAB®. Results are shown in Figure 7, along with the analytical predictions using Eq. (11) (where *I* is divided by *Q* to get the normalized irradiance). A commercial ray-tracing code, ASAP®, was also used to model this system, and the results are shown in Figure 7. In the ray-tracing simulations, up to 20 million rays were used to simulate the irradiance on a small target that was located at different distances from the collector, representative of the observer (camera) locations in the test.

Copyright © 2010 by ASME

Apodization of the source rays was also included to account for sun shape and limb darkening [17].

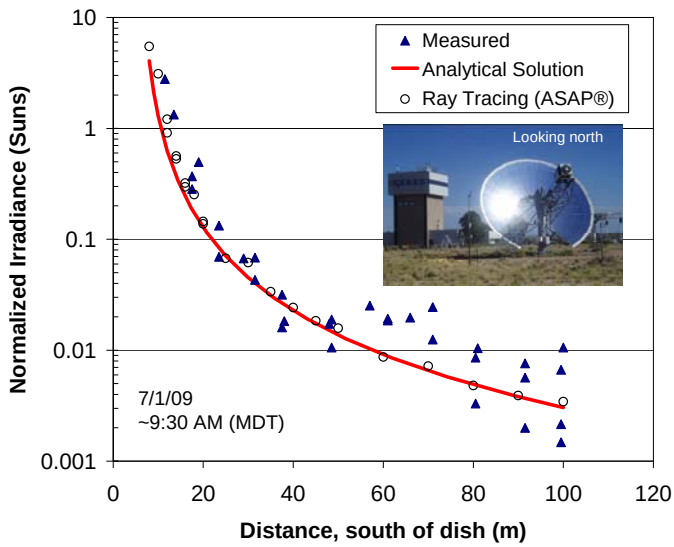

Figure 7. Predicted and measured normalized irradiance as a function of distance caused by specular reflections from the Mod 2-2 10 kW parabolic dish.

The results show that the measured and predicted normalized irradiance from the specularly reflected image of the sun on the dish facets match very well over the range of distances tested. At small distances (within two focal lengths), the normalized irradiance can exceed one sun. At greater distances, the normalized irradiances decrease rapidly due to the diverging beam. It is interesting to note that the analytical solution, which assumes a uniform sun intensity and neglects off-axis aberrations, matches extremely well with the ray-tracing solution, which rigorously includes these effects.

This demonstrates that the analytical solution can be used to give good estimates of the irradiance as a function of distance from the specular reflection. This value, which represents the irradiance at the cornea at a particular distance, can then be used to determine the retinal irradiance for comparison against the safety metrics. For example, at a distance of 40 m, the normalized irradiance is approximately 0.02 suns. From Eq. (13), the subtended angle formed by the reflected image of the sun on the dish is calculated as 1.7 mrad, where I/Q is the normalized irradiance of 0.02 suns, $\rho = 0.93$, and $\beta = 11.4$ mrad. Assuming a direct normal insolation of 0.1 W/cm^2 (equal to one sun), the retinal irradiance is then calculated to be ~5 W/cm^2 using Eqs. (4) and (5) with d_p = 0.002 m, f = 0.017 m, and $\tau = 0.5$. According to Figure 1, a retinal irradiance of 5 W/cm^2 with a subtended angle of 1.7 mrad is less than the safe retinal irradiance metrics to prevent permanent eye damage. However, the calculated irradiance is sufficient to potentially cause a temporary after-image if one were to view directly at the reflected image. Eqs. (3), (11), and (13) yield a minimal distance of 55 m for this system to yield a low potential for after-image effects.

4.2 Diffuse Reflection Tests

The diffuse reflection tests were conducted on July 2, 2009, at approximately 10:00 AM (MDT) with a direct normal insolation of approximately 880 W/m^2. A 147 m^2 ATS heliostat with a reflectivity of ~0.9 was used to concentrate a beam of sunlight onto the front of the NSTTF central receiver tower, which was painted white. The reflection of the sunlight from the front of the painted tower was approximately diffuse. Photos of the beam on the tower were taken at varying distances from the tower, and the images were processed in MATLAB® to determine the normalized irradiance values. Analytical predictions of the irradiance as a function of distance were made using Eq. (19), where the diffuse power emanating from the tower is calculated as the total incident power on the tower times the reflectivity of the tower. The total incident power is calculated as the product of the DNI (880 W/m^2), the surface area of the heliostat (147 m^2), and the cosine loss (0.78) due to the off-axis position of the heliostat (calculated at the date and time of the test), which yields ~100 kW. The total diffusely reflected power, P_d, used in Eq. (19) for hemispherical emission from the front of the tower is equal to the incident power times the reflectivity of the white paint on the tower.

Figure 8 shows the results of the measured and predicted irradiances normalized to the DNI, assuming a reflectivity of the white paint of 0.6. Results show that the measured and predicted irradiances match very closely and follow the same trend as a function of distance from the source. Thus, the analytical solution for diffuse reflections can be used to estimate the irradiance as a function of distance from the diffuse reflection.

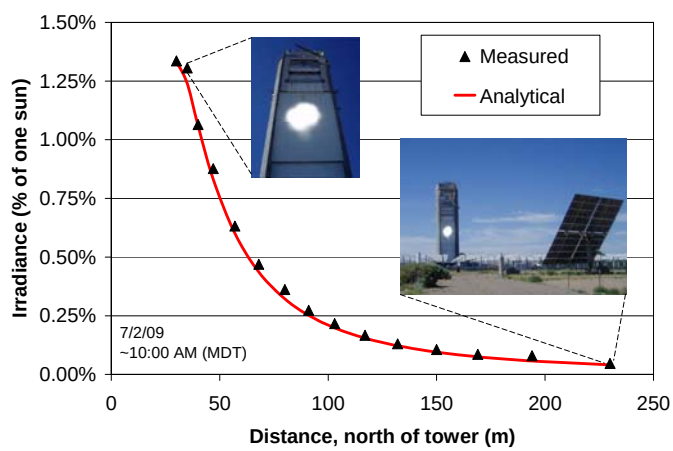

Figure 8. Predicted and measured normalized irradiance as a function of distance caused by diffuse reflections from the NSTTF central receiver tower (painted white, ρ=0.6).

Copyright © 2010 by ASME

5. SUMMARY AND CONCLUSIONS

This paper has presented methods to evaluate potential glint and glare hazards from specularly and diffusely reflected sunlight from concentrating solar collectors. First, a review of metrics used to determine safe retinal irradiances as a function of subtended source angle (or retinal image size) was presented. Metrics for both permanent eye damage and temporary after-image effects were included. Analytical models were then derived to calculate irradiances from both specular and diffuse sources. These models were validated using data collected from specular and diffuse reflection tests.

The methods and equations presented in this paper can be used to calculate irradiances from various concentrating solar collector systems (e.g., heliostats, dishes, troughs, receivers). The calculated retinal irradiance can be compared against the safe retinal irradiance metrics to evaluate potential glint and glare hazards. It should be noted, however, that the quantified metrics and estimates for retinal irradiance do not account for all factors. For example, atmospheric attenuation and the impact of wearing sunglasses are not considered in the models. In addition, human factors and behavior are not assessed in this paper, which may affect the impact of different glint and glare scenarios.

The impact of multiple coincident beams (i.e., from adjacent collectors or receivers) was not considered in this study. Brumleve (pp. 27-32) [1] provides a discussion of the impact of multiple sources that can be used together with the results of this study. In general, multiple sources can increase the retinal image size. In addition, the retinal irradiance may or may not increase depending on whether the projected retinal images overlap, which depends on the positions of the sources relative to the observer. For example, if two beams enter the eye but do not overlap, the affected retinal image area is increased, but the irradiance (W/cm^2) is the same as that from a single beam. If the two beam are nearly coincident and form a coalesced image on the retina, the retinal image size is about the same but the irradiance increases.

Based on the configurations and operation of the various concentrating solar technologies, potential glint and glare scenarios that should be considered include the following:

- Power Towers
  - Specular reflections from heliostats when they are moving to or from stowed position, in standby mode, or are not aimed at the receiver
  - Diffuse reflections from the receiver
- Linear Collectors
  - Specular reflections from the mirrors when they are moving to or from stowed position and from specular reflections off the ends of the trough or mirrors when the sun is low and aligned with the mirrors (e.g., reflections from the north end of a north-south field when the sun is low in the southern horizon)
  - Diffuse and specular reflections from receiver tubes
- Dish/Engine Systems
  - Specular reflections from mirror facets when the dish is off-axis or moving to or from a stowed position
  - Diffuse reflections from the receiver aperture

ACKNOWLEDGMENTS

The authors would like to thank Brian Myer, John Quintana, Kirill Trapeznikov, and Chuck Andraka for their assistance with the dish testing and Matlab image processing. We also thank Siri Khalsa for his assistance compiling and interpreting the safety metrics.

Sandia is a multiprogram laboratory operated by Sandia Corporation, a Lockheed Martin Company for the United States Department of Energy's National Nuclear Security Administration under contract DE-AC04-94AL85000. The publisher, by accepting the article for publication, acknowledges that the United States Government retains a non-exclusive, paid-up, irrevocable, world-wide license to publish or reproduce the published form of this manuscript, or allow others to do so, for United States Government purposes.

REFERENCES

[1] Brumleve, T.D. (1977). Eye Hazard and Glint Evaluation for the 5-MWt Solar Thermal Test Facility, SAND76-8022, Sandia National Laboratories, Livermore, CA.

[2] Brumleve, T.D. (1984). 10 MWe Solar Thermal Central Receiver Pilot Plant: Beam Safety Tests and Analyses, SAND83-8035, Sandia National Laboratories, Livermore, CA.

[3] Sliney, D.H, and Freasier, B.C. (1973). Evaluation of Optical Radiation Hazards, Applied Optics, 12(1), 1-24.

[4] Carrier, J. (2008). Beam Safety Design Parameters, Data Response Attachment DR89-1, Appendix A, Data Response Set 1A. Dated on 1/14/2008, CH2MHILL, Ivanpah Solar Electric Generating System, Application for Certification (07-AFC-5), Submitted to California Energy Commission, http://www.energy.ca.gov/sitingcases/ivanpah/documents/applicant/DR_1a/2008-01-14_ISEGS_DR_SET_1A.PDF.

[5] Carrizo Energy, LLC (2008). Responses to CEC Data Requests (#1-78), Application for Certification (07-AFC-8), Carrizo Energy Solar Farm, Submitted to California Energy Commission, http://www.energy.ca.gov/sitingcases/carrizo/documents/applicant/2008-02-27_DATA_RESPONSES_1-78.PDF.

[6] City of Victorville, (2008). Victorville 2 Hybrid Power Project, Application for Certification (07-AFC-1), submitted to California Energy Commission, www.energy.ca.gov/sitingcases/victorville2/documents/.

[7] San Joaquin Solar 1 & 2 – Application for Certification Volume 2, Appendix L, "Glint and Glare Study," http://www.energy.ca.gov/sitingcases/sjsolar/documents/applicant/afc/AFC_volume_02/.

Copyright © 2010 by ASME

[8] SES Solar Two, LLC (2008). SES Solar Two Project, Application for Certification (08-AFC-5), submitted to California Energy Commission.
[9] Ho, C.K., C.M. Ghanbari, and R.B. Diver (2009). Hazard Analyses of Glint and Glare from Concentrating Solar Power Plants, SAND2009-4131C, in proceedings of SolarPACES 2009, Berlin, Germany, September 15-18, 2009.
[10] Sliney, D.H., (1980). An Evaluation of the Potential Hazards of the Point Focusing Solar Concentrators at the JPL-Edwards Test Site, Report submitted to the Jet Propulsion Laboratory (JPL Consulting Agreement No. JF 714696), California Institute of Technology, Pasadena, CA.
[11] Delori, F.C., R.H. Webb, and D.H. Sliney, (2007). Maximum permissible exposures for ocular safety (ANSI 2000), with emphasis on ophthalmic devices, J. Opt. Soc. Am. A, 24(5), 1250-1265.
[12] Metcalf, R.D and R.E. Horn, (1958).Visual Recovery Times from High-Intensity Flashes of Light, Air Force Aerospace Medical Research Lab, Wright Air Development Center Technical Report 58232.
[13] Severin, S.L. N.L. Newton, and J.F. Culver, (1962). An Experimental Approach to Flash Blindness, Aerospace Medicine, 1199-1205.
[14] Saur, R.L. and S.M. Dobrash, (1969). Duration of Afterimage Disability after Viewing Simulated Sun Reflections, Applied Optics, 8(9), 1799-1801.
[15] Duffie, J.A. and W.A. Beckman, (1991) Solar Engineering of Thermal Processes, 2nd Ed., John Wiley & Sons, Inc., New York.
[16] Diver, R.B., C.E. Andraka, K.S. Rawlinson, T.A. Moss, V. Goldberg, and G. Thomas, Status of the Advanced Dish Development System Project, Proceedings of ISEC 2003, 2003 ASME International Solar Energy Conference, Hawaii, March 15-18, 2003.
[17] Rabl, A. and P. Bendt (1982). Effect of Circumsolar Radiation on Performance of Focusing Collectors, J. Solar Energy Engr., 104, 237-250.

Copyright © 2010 by ASME